Reducing the stray light of holographic gratings by shifting the substrate a short distance in the direction parallel or perpendicular to the exposure interference fringes

Donghan Ma (马冬晗) and Lijiang Zeng (曾理江)*

Department of Precision Instrument, State Key Laboratory of Precision Measurement Technology and Instruments, Tsinghua University, Beijing 100084, China

**Corresponding author: zenglj@tsinghua.edu.cn*

Received April 20, 2017; accepted June 6, 2017; posted online June 30, 2017

This research proposes a simple and practical method to make low-stray-light gratings, where the substrate shifts about a 1 mm distance in the direction parallel or perpendicular to the exposure interference fringes. When the substrate shifts, a reference grating next to the substrate is used to adjust in real time the phase of the exposure interference fringes relative to the substrate. Shifting eliminates the exposure defects and therefore decreases the stray light of gratings. Several gratings are successfully made by using this method, which have straighter grooves, smoother surfaces, and lower stray light than gratings made in conventional interference lithography.

OCIS Codes: 050.1950, 050.2770, 290.2648, 290.5880.

doi: 10.3788/COL201715.100501.

Diffraction gratings are widely used in many fields including spectral analysis[1–3], precision metrology[4–6], and chirped-pulse-amplification systems[7–9]. The main procedures to fabricate a grating consist of photoresist spin-coating, holographic exposure, development, and ion-beam etching. In conventional holographic exposure, the defects of the interference field, such as the laser speckles and the defects of the optical elements, are recorded in the photoresist, resulting in curved grating lines, rough surface, and stray light[10]. How to solve this problem and obtain low-stray-light gratings is attractive and challenging. For the photoresist mask fabrication process, Li *et al.* proposed to make low-stray-light gratings via suppressing the interface reflections by means of antireflective coatings in near-field holography[11]. Yu *et al.*[12] and Rabady *et al.*[13] separately proposed to reduce the mask defects and get smooth grooves by heat-treating the photoresist mask. For the ion-beam etching process, some researchers utilized the off-cut silicon wafers for wet etching to fabricate silicon immersion gratings applied in astronomical spectrometers[14–16]. Steiner *et al.* rendered that blazed gratings of lower stray light could be obtained by using normal etching after asymmetrical exposure than by using conventional oblique etching after symmetrical exposure[17]. Lin *et al.* proposed to remove the mask irregularities by utilizing the ashing effect of O^+ ions during etching[18]. Tan *et al.* presented an inductively coupled plasma etching–polishing method. They first used CHF_3-SF_6 mixed gas to etch a preliminary grating profile, and then used Ar-O_2 mixed gas to polish the gratings and, thus, obtained low surface roughness[19].

Among all these proposed methods, improving the quality of the photoresist mask during exposure is a more direct approach to make low-stray-light gratings. In 2015, we proposed broad-beam scanning exposure to eliminate the high-frequency defects of the interference field[20]. In this method, the substrate passed through the exposure interference field at a constant speed along the grating vector (in the direction perpendicular to both the grating grooves and the substrate normal, the same below), and, hence, the defects were averaged by the scanning exposure. Although this method shows a good effect to reduce the stray light of gratings, it has two drawbacks. First, it takes a much longer time to make a grating in scanning exposure than conventional holographic exposure. Second, the substrate needs to move a several-centimeter distance during scanning, so a large-area reference grating is required for phase and attitude locking.

In this Letter, we present a simple method for making low-stray-light gratings, where the substrate shifts about a 1 mm distance in the direction parallel or perpendicular to the exposure interference fringes. When the substrate shifts, a small-area reference grating next to the substrate is used to adjust in real time the phase of the exposure interference fringes relative to the substrate. This method maintains the effects of scanning exposure, while overcoming the aforementioned drawbacks. It is expected to be a convenient and practical approach to make low-stray-light gratings.

Figure 1 schematically depicts the optical layout of the exposure system. When the shutter K is opened, the laser beam is divided by the polarizing beam splitter (PBS) into two beams, whose intensities and polarization states can be adjusted by the half-wave plates WP_1 and WP_2. The transmitted beam B_1 is reflected by the mirror M_1, modulated by the acoustic optical modulator AOM_1, cleaned up by the spatial filter SF_1, and then collimated by the lens L_1. Similarly, the reflected beam B_2 is modulated by

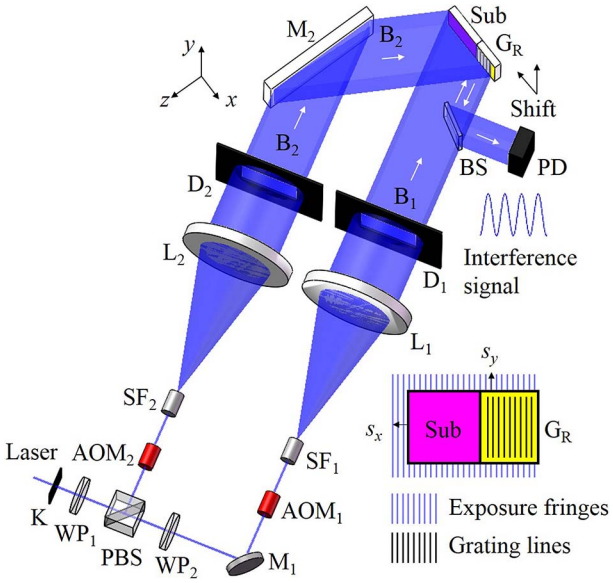

Fig. 1. Optical layout of the exposure system. L_{1-2}, collimating lens; Sub, photoresist-covered substrate.

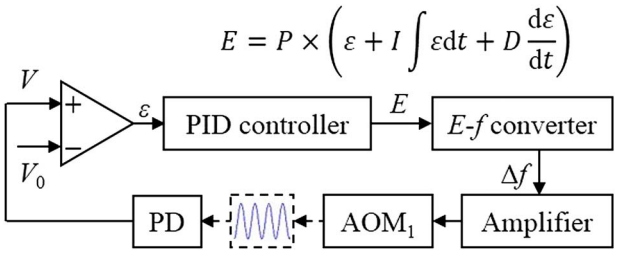

Fig. 2. Phase locking loop.

AOM_2, cleaned up by SF_2, collimated by L_2, and then reflected by the mirror M_2. The diaphragms D_1 and D_2 are used to limit the collimated beams B_1 and B_2 to have rectangular cross sections, respectively. B_1 and B_2 generated interference fringes on the photoresist-covered substrate for exposure.

Different from conventional holographic exposure, in this system, the substrate Sub, together with a prefabricated reference grating G_R, is mounted on a motorized translation stage (not shown in Fig. 1). We define the x, y, and z axes as along the directions of grating vector, grating grooves, and normal of the substrate surface, respectively. During exposure, the translation stage carries Sub and G_R together to shift about a 1 mm distance at a constant speed along the x or y axis. In this way, the high-frequency defects of the exposure interference field can be averaged, and, thus, the stray light of gratings can be reduced.

To avoid fringe smearing, the exposure interference fringes should be kept stationary relative to the shifting substrate, which is realized by utilizing G_R. As shown in Fig. 1, the +1st order of the transmitted part of B_1 from the beam splitter (BS) and the 0th order of B_2, both diffracted by G_R, form an interference signal, which is reflected by the BS and then detected by the photoelectric detector (PD). The phase of the interference signal can reflect the phase of the exposure interference fringes relative to the substrate, so it should be locked during exposure. We use the PD to detect the intensity V of the interference signal, and then compare V with the target value V_0. As shown in Fig. 2, if there exists $\varepsilon = V - V_0 \neq 0$, the proportion-integration-differentiation (PID) controller outputs a feedback voltage E. E is then converted to a frequency signal Δf to change the carrier frequency of AOM_1 for phase compensation until ε is sufficiently small that it cannot be distinguished[20]. Consequently, the exposure interference fringes are "frozen" on the shifting substrate.

Due to the angular errors of the translation stage, when the substrate shifts, its attitude may change[21]. We define $\Delta\theta_x$, $\Delta\theta_y$, and $\Delta\theta_z$ as rotation angles of the substrate about the grating vector, the grating grooves, and the normal of the substrate surface, respectively. The rotation $\Delta\theta_x$ has no influence on the exposure effects. The rotation $\Delta\theta_y$ leads to a period variation of the interference fringes recorded in the photoresist. The rotation $\Delta\theta_z$ results in a direction tilt of the interference fringes recorded in the photoresist. Fortunately, since the shifting distance is only about 1 mm, $\Delta\theta_y$ and $\Delta\theta_z$ are both within 0.2 arcsec, whose influences on the exposure effects can be neglected.

In experiments, the exposure light source was a semiconductor laser (Toptica SYST TopMode 405) with a wavelength of 405 nm, a power of 100 mW, and a coherence length of larger than 25 m. The collimating lenses were plano-convex lenses with a focus length of 500 mm and an aperture diameter of 100 mm. The motorized stage (Suruga KS102-100) had a translation range of 100 mm, a pitch angle of 25 arcsec, and a yaw angle of 20 arcsec in the whole range. The PD (Newport 2001-FS-M) had a bandwidth of 200 kHz and a rise time of 2 μs. The PID controller (SRS SIM960) had a bandwidth of 100 kHz and an output resolution of 1 mV. Positive photoresist (Shipley S9912) was used. The reference grating G_R was prefabricated in this exposure system with a period of 574.7 nm. Gratings were made on glass slides with a size of 35 mm × 40 mm. To enhance the adhesiveness of the photoresist, a 120-nm-thick chromium film was coated on the slides.

We did three sets of experiments to demonstrate the effectiveness of this method. Since the shifting distance determines the amount of exposure interference fringes to be averaged in this method, we studied the effects of different shifting distances to decrease the stray light in the first set of experiments. Meanwhile, we studied the influences of the photoresist thickness and the shifting direction in the second and third sets of experiments, respectively. In experiments, the duty cycle (the ratio of the linewidth to the grating period) was mainly determined by the exposure dose and the development time[22]. Moreover, if fringe smearing exists during exposure, the duty cycle will decrease obviously. To estimate the

exposure effects, we observed the microstructures of the fabricated gratings under the scanning electron microscope (SEM), and observed the surface appearances under the low-magnification microscope (5× objective). Then, we observed the stray light of the gratings fabricated in different conditions for a comprehensive comparison.

In the first set of experiments, the photoresist thickness was approximately 140 nm, the exposure time was 25 s, and the shifting direction was along the grating vector. Several gratings were fabricated with different shifting distances, whose microstructures are shown in Figs. 3(a)–3(d), and surface appearances are shown in Figs. 4(a)–4(d). It is seen that in stationary exposure (the shifting distance $s = 0$), the grating grooves are curved [Fig. 3(a)], and the surface is rough, like orange peels [Fig. 4(a)]. As s increases, the grating grooves become straighter [Figs. 3(b)–3(d)], and the surfaces become smoother [Figs. 4(b)–4(d)]. When s increases to 0.1 mm, the grating grooves are straight enough, and the surface roughness is sufficiently eliminated and is sub-equal to that of the bare substrate [Fig. 4(e)]. The duty cycles of the gratings are similar, meaning that no fringe smearing existed.

In the second set of experiments, the photoresist thickness was approximately 250 nm, the exposure time was 50 s, and the shifting direction was along the grating vector. Similarly, several gratings were made with different shifting distances, as shown in Figs. 5 and 6. We can see that when the photoresist thickness increases, a shifting distance of 0.1 mm is still sufficient to improve the straightness of the grating lines and the smoothness of the grating surfaces.

In the third set of experiments, the photoresist thickness was approximately 250 nm, the exposure time was 50 s, and the shifting direction was along the grating grooves. Several gratings were made with different shifting distances, as shown in Figs. 7 and 8. It is seen that the exposure effect is also similar when the shifting direction is along the grating grooves. However, since the exposure defects have different frequencies in these two directions, in this direction, a shifting distance of 0.4 mm is sufficient to obtain gratings with a smooth surface and straight grating lines.

From these three sets of experiments, we can see that as long as the substrate shifts within a 1 mm distance in the direction parallel or perpendicular to the exposure interference fringes, the straightness of the grating lines and the smoothness of the grating surfaces can be well improved.

Then, we set up an optical path to observe the stray light of the fabricated gratings, as shown in Fig. 9. The laser with a wavelength of 405 nm illuminated the grating

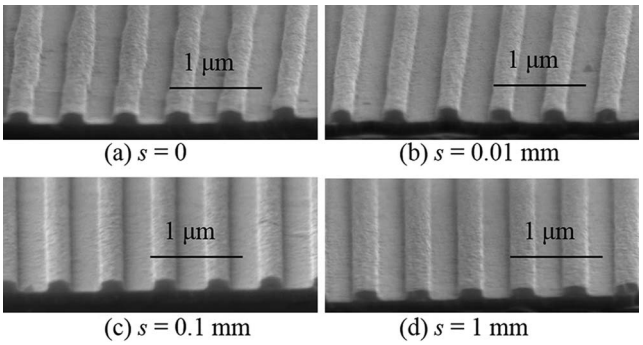

Fig. 3. SEM photographs of the gratings made when (a) $s = 0$, (b) $s = 0.01$ mm, (c) $s = 0.1$ mm, and (d) $s = 1$ mm.

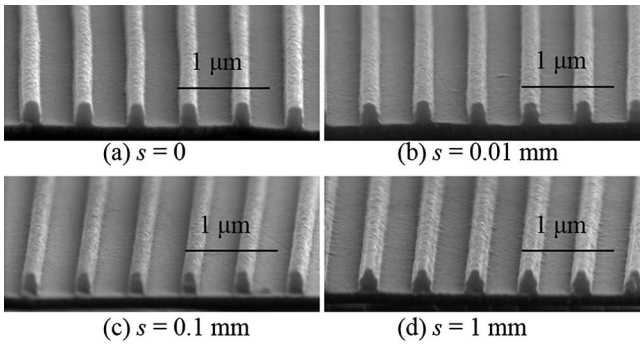

Fig. 5. SEM photographs of the gratings made when (a) $s = 0$, (b) $s = 0.01$ mm, (c) $s = 0.1$ mm, and (d) $s = 1$ mm.

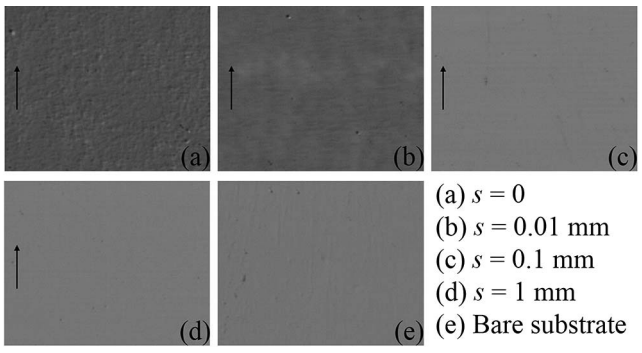

Fig. 4. Surface appearances of the gratings made when (a) $s = 0$, (b) $s = 0.01$ mm, (c) $s = 0.1$ mm, (d) $s = 1$ mm, and (e) the bare substrate. The arrowheads show the direction of the grating grooves.

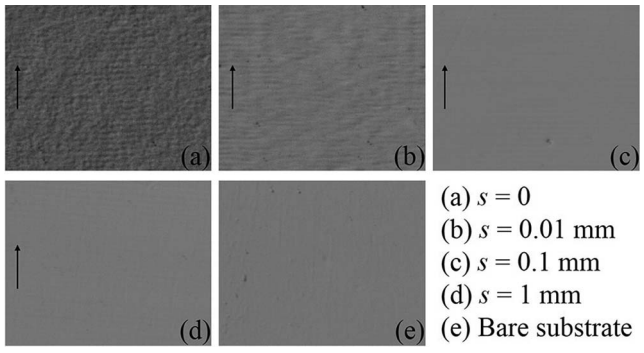

Fig. 6. Surface appearances of the gratings made when (a) $s = 0$, (b) $s = 0.01$ mm, (c) $s = 0.1$ mm, (d) $s = 1$ mm, and (e) the bare substrate. The arrowheads show the direction of the grating grooves.

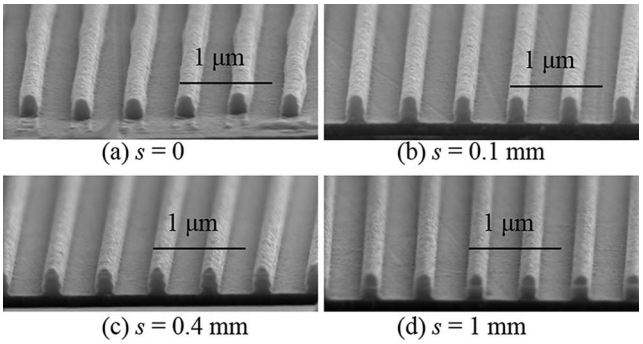

Fig. 7. SEM photographs of the gratings made when (a) $s = 0$, (b) $s = 0.1$ mm, (c) $s = 0.4$ mm, and (d) $s = 1$ mm.

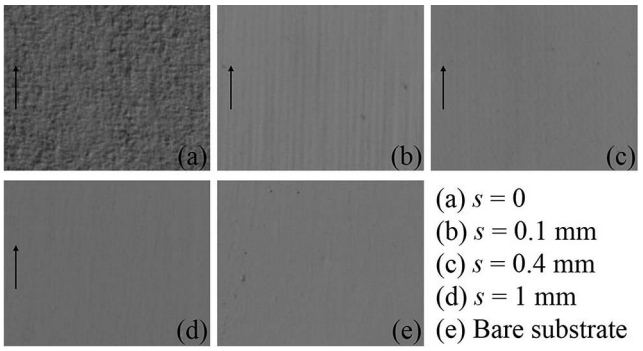

Fig. 8. Surface appearances of the gratings made when (a) $s = 0$, (b) $s = 0.1$ mm, (c) $s = 0.4$ mm, (d) $s = 1$ mm, and (e) the bare substrate. The arrowheads show the direction of the grating grooves.

at normal incidence. A glass wafer coated with a chromium film disk area in the middle, whose diameter was 2 mm larger than the laser beam diameter, was employed to separate the stray light from the main diffraction spots. The main part of the first-order diffraction beam of the grating was reflected by the disk area, and the transmitted residual part, i.e., the stray light, was projected onto a screen and then recorded by a CCD camera with a fixed exposure time and gain, as shown in Fig. 10. It states that the grating made in stationary exposure has some stray

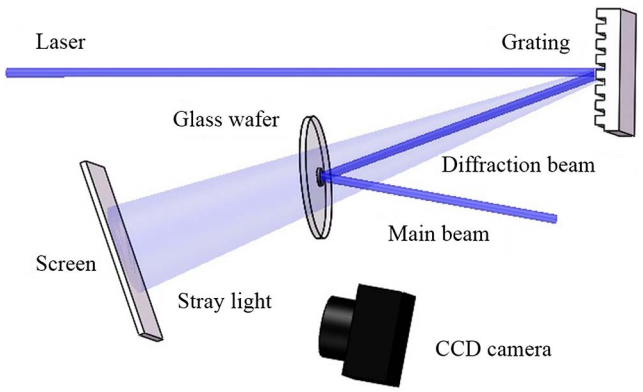

Fig. 9. Optical path to observe the stray light of gratings.

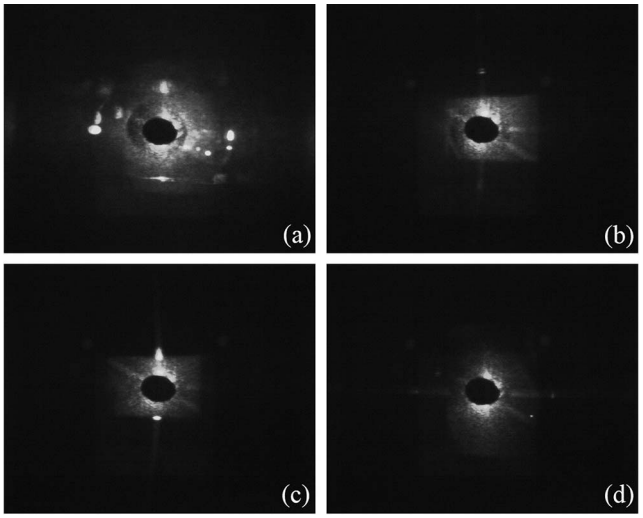

Fig. 10. Stray light of gratings. (a) $s = 0$, and the photoresist thickness was 250 nm. (b) $s = 0.1$ mm, the photoresist thickness was 140 nm, and shifting was along the grating vector. (c) $s = 0.1$ mm, the photoresist thickness was 250 nm, and shifting was along the grating vector. (d) $s = 0.4$ mm, the photoresist thickness was 250 nm, and shifting was along the grating grooves. The light spots were recorded by the CCD camera with the same exposure time and gain.

light around the main light spot [Fig. 10(a)], while the diffraction light spots of the gratings made in shifting exposure are very clean [Figs. 10(b)–10(d)].

We calculated the average gray values of the images in Fig. 10 and divided them by the saturated value 255. The results were used to describe the stray-light levels of the gratings, as shown in Table 1. Meanwhile, we measured the first-order diffraction efficiencies of the gratings for reference. It states that the shifting exposure can reduce the stray-light levels by 30%–40%, while the diffraction efficiencies have no obvious difference.

These experimental results prove that this method is applicable to making low-stray-light gratings. Some essential supplements are as follows:

First, if the shifting direction is along the grating grooves, the phase variation during shifting is generally within several grating periods. We can use a piezoelectric transducer attached to the back of M_1 instead of the AOM_1 for phase compensation. Then, the exposure system becomes simpler and lower-cost.

Second, if the angular errors of the translation stage are very large and cannot be omitted, we can use attitude locking to eliminate their influences on the exposure effects. More details can be found in Ref. [20].

Third, if the grating period d_R of G_R and the exposure wavelength λ_{exp} satisfy $d_R > 1.5\lambda_{exp}$, the +2nd order of B_1 diffracted by G_R exists. The +2nd order of B_1 and the +1st order of B_2, both diffracted by G_R, generate the interference signal, which is directly detected by the PD for phase locking. Then, the BS is no longer needed.

In conclusion, we propose a simple method to reduce the stray light of holographic gratings. During exposure, the

Table 1. Stray Light Levels

Description	Efficiency (%)	Stray-light Level	Reduction Factor (%)
$s = 0$, $h = 250$ nm[a]	11.0	0.1433	–
$s = 0.1$ mm, $h = 140$ nm, shifting along the x axis	12.9	0.0961	32.9
$s = 0.1$ mm, $h = 250$ nm, shifting along the x axis	10.8	0.0865	39.6
$s = 0.4$ mm, $h = 250$ nm, shifting along the y axis	10.6	0.0862	39.8

[a]h, photoresist thickness.

substrate shifts about a 1 mm distance in the direction parallel or perpendicular to the interference fringes. In this way, the high-frequency defects of the exposure interference field are averaged, and, therefore, the stray light of the gratings can be decreased. Several gratings are successfully made by using this method, which have straighter grating lines, smoother surfaces, and lower stray light than gratings made in the conventional exposure method. This is a convenient and practical approach to make low-stray-light gratings.

This work was supported by the National Natural Science Foundation of China under Grant No. 51427805.

References

1. G. Fortin and N. McCarthy, Appl. Opt. **44**, 4874 (2005).
2. T. Glaser, Adv. Opt. Technol. **4**, 25 (2015).
3. Q. Zhou, J. Pang, X. Li, K. Ni, and R. Tian, Chin. Opt. Lett. **13**, 110501 (2015).
4. J. Carr, M. Y. P. Desmulliez, N. Weston, D. McKendrick, G. Cunningham, G. McFarland, W. Meredith, A. McKee, and C. Langton, Precis. Eng. **33**, 263 (2009).
5. A. Kimura, W. Gao, A. Yoshikazu, and L. Zeng, Precis. Eng. **34**, 145 (2010).
6. X. Li, H. Wang, K. Ni, Q. Zhou, X. Mao, L. Zeng, X. Wang, and X. Xiao, Opt. Express **24**, 21378 (2016).
7. T. J. Kessler, J. Bunkenburg, H. Huang, A. Kozlov, and D. D. Meyerhofer, Opt. Lett. **29**, 635 (2004).
8. F. Canova, O. Uteza, J. P. Chambaret, M. Flury, S. Tonchev, R. Fechner, and O. Parriaux, Opt. Express **15**, 15324 (2007).
9. F. Kong, Y. Jin, S. Liu, S. Chen, H. Guan, K. He, Y. Du, and H. He, Chin. Opt. Lett. **11**, 102302 (2013).
10. E. K. Popov, L. V. Tsonev, and M. L. Sabeva, Opt. Eng. **31**, 2168 (1992).
11. Y. Li, H. Chen, S. Kroker, T. Käsebier, Z. Liu, K. Qiu, Y. Liu, E. B. Kley, X. Xu, Y. Hong, and S. Fu, Chin. Opt. Lett. **14**, 090501 (2016).
12. Z. Yu, L. Chen, W. Wu, H. Ge, and S. Y. Chou, J. Vac. Sci. Technol. B **21**, 2089 (2003).
13. R. Rabady, D. Frankstein, and I. Avrutsky, Opt. Lett. **28**, 1665 (2003).
14. J. P. Marsh, D. J. Mar, and D. T. Jaffe, Appl. Opt. **46**, 3400 (2007).
15. W. Wang, M. Gully-Santiago, C. Deen, D. J. Mar, and D. T. Jaffe, Proc. SPIE **7739**, 77394L (2010).
16. J. Ge, B. Zhao, S. Powell, A. Fletcher, X. Wan, L. Chang, H. Jakeman, D. Koukis, D. B. Tanner, D. Ebbets, J. Weinberg, S. Lipscy, R. Nyquist, and J. Bally, Proc. SPIE **8450**, 84502U (2012).
17. R. Steiner, A. Pesch, L. H. Erdmann, M. Burkhardt, A. Gatto, R. Wipf, T. Diehl, H. J. P. Vink, and B. G. Bosch, Proc. SPIE **8870**, 88700H (2013).
18. H. Lin, L. Zhang, L. Li, C. Jin, H. Zhou, and T. Huo, Opt. Lett. **33**, 485 (2008).
19. X. Tan, Q. Jiao, X. Qi, and H. Bayan, Opt. Express **24**, 5896 (2016).
20. D. Ma and L. Zeng, Opt. Lett. **40**, 1346 (2015).
21. L. Shi, L. Zeng, and L. Li, Opt. Express **17**, 21530 (2009).
22. L. Li, M. Xu, G. I. Stegeman, and C. T. Seaton, Proc. SPIE **835**, 72 (1987).